A Slow Pyrolysis Biochar Derived from *Tetrapanax papyriferum* Petiole as an Effective Sorbent for Removing Copper ions from Aqueous Solution

Wenqi Li,[a,#] Liping Zhang,[a,#] Ying Guan,[a] Zhihan Tong,[b] Xiang Chen,[a] Guanqiao He,[a] and Hui Gao [a,*]

Biochar derived from *Tetrapanax papyriferum* petioles at different pyrolysis temperatures was used to remove copper from aqueous solution. Abundant porous structures were observed with scanning electron microscopy, and transmission electron microscope images revealed a unique layered nanopore structure. A high pyrolytic temperature resulted in a biochar with a higher surface area, ash content, and mineral element content. The maximum adsorption capacity of *T. papyriferum* petiole biochar (TBC) was 182 mg/g. The Langmuir adsorption isotherm model and pseudo-second-order kinetics model were most suitable for describing the adsorption process, indicating that adsorption takes place at specific homogeneous sites within the adsorbent. The calculated $\Delta H°$ values indicated that the adsorption process was endothermic. The adsorption mechanism for TBC was attributed to precipitation, ion exchange, C-π interactions, and complexation. Thus, the biochar used in this study is a promising environmentally friendly and effective adsorbent for removing Cu^{2+} ions from an aqueous solution.

Keywords: Tetrapanax papyriferum; Biochar; Heavy metals; Adsorption; Isotherms

*Contact information: a: School of Forestry and Landscape Architecture, Anhui Agricultural University, Hefei 230036, China; b: College of Materials Science and Engineering, Northeast Forestry University, Harbin 150040, China; *Corresponding author: huigaozh@163.com*
#: These authors contributed equally to this study.

INTRODUCTION

Tetrapanax papyriferum (Family: Araliaceae) is native to northern Formosa and to the South China provinces of Hunan, Szechwan, Yunnan, Kweichow, Kwangsi, and Kwangtung. Under natural conditions, it is usually a shrub 3.0 to 6.0 feet tall but may attain a height of 30.0 feet (Ho *et al.* 2005). *Tetrapanax papyriferum* has large leaves. The diameter of the lamina is 55.0 ± 1.1 to 85.0 ± 1.2 cm, and the average length and diameter of its petiole is 70.0 ± 2.0 to 90.0 ± 3.5 cm and 0.8 ± 0.2 to 1.6 ± 0.4 cm, respectively. The petiole of *T. papyriferum* is hollow, and a white layer lies close to the inner wall. Furthermore, *T. papyriferum* has many special characteristics, such as low wood density, extremely fast growth, short felling period, wide adaptability, and strong self-reproduction ability. However, far too little attention has been paid to its potential applications. *Tetrapanax papyriferum* is inefficiently used and is not recycled. It has even been considered an invasive species in some places. In China, the stalk pith of *T. papyriferum* is a famous traditional Chinese medicine that is produced annually, but the leaves are discarded, resulting in serious waste. The comprehensive utilization of *T. papyriferum*, including its lamina and stalk, has become an increasingly challenging issue.

Large quantities of heavy metal ions bioaccumulate throughout the food chain,

where they threaten human health (Mishra *et al*. 2012; Lin *et al*. 2017b; Teodoro *et al*. 2017). Copper is an essential trace element that is not easily degraded. Many diseases, such as stomach and intestinal disorders, occur in humans when copper is ingested in excess (Lin *et al*. 2017a). Thus, efficient techniques are necessary to eliminate heavy metal ions from wastewater. There are many techniques for removing heavy metal ions (Lin *et al*. 2017a; Niu *et al*. 2017; Ren *et al*. 2017), including physical, chemical, and biological methods, such as chemical precipitation, ion exchange, adsorption, membrane filtration, and solvent extraction. Data from several studies suggests that adsorption is a highly efficient, cost-effective, and simple technique to remove heavy metal ions with minimal production of secondary pollution (Zhang *et al*. 2018a, b).

The most widely used class of adsorbents is carbon-based absorbents. Biochar (BC) is a carbon-rich solid derived from the thermal degradation of plant residue and agricultural waste in an oxygen-limited environment (Vyavahare *et al*. 2018). Biochar has been prepared from various feedstock materials, such as wood, sugarcane, rice husk, bamboo, dairy manure, and bioenergy residue (Li *et al*. 2017; Xu *et al*. 2017; Vyavahare *et al*. 2018). A great deal of research on biochar has focused on its adsorption of heavy metal ions (Han *et al*. 2016; Park *et al*. 2016; Qian *et al*. 2016). Idrees *et al*. (2018) used guinea fowl manure derived biochar and cattle manure derived biochar to adsorb Cu^{2+} ions, and the maximum sorption capacity values were 46.6 and 44.5 mg/g, respectively. Zhou *et al*. (2017) investigated the adsorption of Cu^{2+} ions using biochar derived from earthworm manure at different pyrolysis temperatures. The adsorption capacity was 24.27 mg/g. Kim *et al*. (2016) prepared KOH-activated *Enteromorpha compressa* biochars to investigate the removal efficiency of Cu^{2+} ions from an aqueous solution. The adsorption capacity of Cu^{2+} ions was 137 mg/g. Biochar is a low-cost adsorbent with high specific surface area and a high capacity to adsorb heavy metal ions. Thus, biochar is a promising alternative agent for removing heavy metal ions. The adsorption capacity of a biochar depends highly on its physicochemical properties, such as surface area, pore properties, and elemental constitution. The physicochemical properties of a biochar depend upon the raw material, pyrolysis temperature, environment (limited oxygen or N_2), and the heating rate. Hence, selection of the feedstock and pyrolysis conditions has an important impact on the final sorption properties of a biochar.

Tetrapanax papyriferum grows and reproduces at a very high rate and is considered an invasive plant species in some locations. No previous study has investigated adsorption of heavy metal ions using a biochar derived from *T. papyriferum*. Thus, this inexpensive and readily available waste biomass was used to remove Cu^{2+} ions from wastewater. In this study, a new low-cost biochar adsorbent derived from *T. papyriferum* petioles was prepared at different temperatures and used to remove Cu^{2+} ions. This study evaluated the absorption behavior of Cu^{2+} ions in *T. papyriferum* petiole biochar (TBC) under different pyrolysis conditions. The biochars were characterized *via* elemental analysis, the Brunauer-Emmett-Teller (BET) method, Fourier transform infrared spectroscopy (FT-IR), X-ray diffraction (XRD), scanning electron microscopy (SEM), X-ray photoelectron spectrometry (XPS), transmission electron microscopy (TEM), and atomic absorption spectroscopy (AAS). Batch experiments were conducted for different factors, such as initial pH, contact time, concentration of Cu^{2+} ions, and temperature.

EXPERIMENTAL

Materials

Tetrapanax papyriferum was planted at Anhui Agricultural University (Anhui, China), and its petioles were used as the raw material in this study. The mature petioles of *T. papyriferum* were harvested, cleaned, air-dried, and cut into 5 cm lengths for the biochar samples. $CuSO_4 \cdot 5H_2O$ was purchased from Sinopharm Chemical Reagent Co., Ltd. (Shanghai, China). Deionized water (18 $M\Omega \cdot cm^{-1}$) was prepared using a Milli-Q purification system from Kertone (Changsha, China).

Methods

Preparation of the biochars

The air-dried samples were pyrolyzed in a tubular vacuum furnace (BTF-1200C-II, BEQ, Anhui, China) under a N_2 atmosphere. The samples were heated from room temperature to 500, 600, 700, or 800 °C at a rate of 5 $°C \cdot min^{-1}$, and the temperature was held for 2 h. The temperature of the samples decreased to room temperature at a rate of 5 $°C \cdot min^{-1}$. Finally, the biochars were sieved through 200 mesh. The resulting biochars were named TBC-500, TBC-600, TBC-700, and TBC-800.

Characterization of the biochars

C, H, and N contents were measured with a CHN Elemental Analyzer (Vario EL Cube, Elementar, Langenselbold, Germany). The percentage of oxygen in each sample was estimated by mass difference (100% minus the percent of C, H, N, and ash). The biochar ash was obtained by heating the samples to 800 °C for 2 h in a muffle furnace (Wang *et al*. 2016). The elemental contents (*e.g.*, Ca, Mg, Fe, K, Cu, Mn, and Zn) were analyzed using AAS (TAS-990, Pgeneral, Beijing, China) (Tong *et al*. 2011). The surface areas of the biochars were measured with a surface area analyzer (BET, ASAP20, Micromeritics Inc., Norcross, GA, USA) using the N_2 adsorption method. The FT-IR spectra of the samples were measured with a Nicolet 6670 spectrometer (Thermo Fisher, Waltham, MA, USA) in the range of 4,000 to 400 cm^{-1} with a resolution of 2 cm^{-1}. The XRD measurements were performed with an XRD-3 diffractometer (PERSEE, Beijing, China) using Cu Kα radiation and an X-ray wavelength of 0.15406 nm at 36 KV and 20 mA. X-ray photoelectron spectrometry (XPS) data was obtained with an ESCALAB 250Xi electron spectrometer (Thermo Fisher). The morphology of each sample was observed *via* field emission SEM (S-4800, Hitachi, Tokyo, Japan) with the samples being sputter coated with gold. Several drops of the diluted suspension were deposited onto a freshly cleaved mica substrate and allowed to dry. Dispersibility of the biochar was investigated by TEM using the HT7700 (Hitachi, Japan) instrument. The pH of each sample was measured with a pH meter (Rex PHS-25, Shanghai, China) at a ratio 1:20 (m/V, g/mL) sample: water.

Batch adsorption experiments

A 1,000 mg/L solution of Cu^{2+} ions was prepared by accurately dissolving weighed $CuSO_4 \cdot 5H_2O$ in distilled water, and other experimental solutions were obtained by dilution. The concentration of Cu^{2+} ions was determined by AAS (TAS-990, Pgeneral, Beijing, China). Batch adsorption experiments were performed to remove the Cu^{2+} ions from a 15 mL solution of Cu^{2+} ions. The initial pH of the heavy metal solution was adjusted using 0.1 M HCl and 0.1 M NaOH solutions. A 15 mL aliquot of Cu^{2+} ion

solution was mixed with 40 mg of adsorbent in a 50 mL centrifuge tube and shaken at 180 rpm and 30 °C. The effects of initial metal ion concentration (25 to 1,000 mg/L, adsorption time 24 h) and contact time (10 to 120 min) on adsorption performance were investigated in the batch mode of operation. The effects of various temperatures on the removal capacity of the adsorbent were also studied.

The amount of heavy metal adsorbed per unit mass of the adsorbent (Q_e) was calculated using the following mass balance equation,

$$Q_e = (C_0\text{-}C_e) \times (V/m) \quad (1)$$

where C_0 and C_e are the initial and equilibrium concentrations of Cu^{2+} ions (mg/L), respectively; V is the volume of solution (L); m is the weight of the dry biochars (g); and Q_e is the adsorption capacity of the adsorbent for Cu^{2+} ions (mg/g).

Reutilization of TBC biochar

Briefly, in the first sorption cycle, 40 mg of the adsorbent was mixed with 15 mL of 150 mg/L (pH = 5) Cu^{2+} ion solution and shaken at 30 °C for 12 h. The successfully adsorbed Cu^{2+} ions from the first cycle were separated with a 0.45 μm filter and washed with distilled water. After drying, the adsorbent was reutilized for the next three cycles of Cu^{2+} ion sorption. This experiment investigated the recycling performance of the TBC.

RESULTS AND DISCUSSION

Characterizations of the Biochars

The SEM and TEM images of the biochars are presented in Fig. 1. An abundant number of pores was detected in the structures in Fig. 1, but the pore structures and pore sizes were irregular and heterogeneous. The TEM images of TBC provided further detailed structural information, revealing a unique stacked and multi-layered morphology with a layered nanopore structure and bulky aggregation. Undoubtedly, the pore structure provided more usable surface area causing higher adsorption of heavy metals.

The nitrogen adsorption-desorption isotherms and the pore size distribution of the biochars are shown in Fig. 2. The N_2 adsorption-desorption can provide preliminary qualitative information on the adsorption mechanism and on the porous structure of the carbons. Figure 2 shows a representative N_2 adsorption-desorption isotherm and the corresponding Barrett-Joyner-Halenda (BJH) pore size distribution curve. The adsorption-desorption isotherm plot of TBC-500 and TBC-600 represents a Type III (non-porous multi-layer adsorption) isotherm. The BET surface areas of the TBC-600 and TBC-500 were 3.82 and 1.81 m^2/g, respectively. The isotherm plot of TBC-700 shows a hysteresis which implies the existence of the open channel in biochar structure. For the TBC-700, the N_2 isotherms were of type IV, with type-H_4 hysteresis loops, which implies the existence of micro- and mesoporous structures in the TBC-700, and narrow cracks and pores in the sorbent materials. Then the isotherm plot of TBC-800 resembles Type II isotherm (non-porous, mono to multi-layer adsorption). The Type II sorption curves are associated with micro and mesoporous solids. The fast-growing nitrogen adsorption curves indicated molecular monolayer adsorption or microporous multilayer adsorption. The surface area was dramatically increased from 1.81 m^2/g to 236.4 m^2/g when the pyrolysis temperature was increased to 800 °C, indicating an increase in the extent of raw material cracking and gradual development of the pore structure. The BET surface areas

of the TBC (800, 700, 600, and 500) were 236.4, 207.3, 3.8, and 1.8 m^2/g, respectively. The BET surface area of TBC increased sharply from 1.8 (500 °C) to 236.4 m^2/g (800 °C), indicating that a well-developed porous structure formed at the higher pyrolysis temperatures. The pore volumes of the biochars were 0.177, 0.164, 0.038, and 0.023 cm^3/g for TBC-800, TBC-700, TBC-600, and TBC-500, respectively. The mean pore sizes of the biochars were 1.50, 3.24, 40.0, and 51.2 nm for TBC-800, TBC-700, TBC-600, and TBC-500, respectively. The pore diameter indicated that microspores and mesospores were the main porous structures in the biochars. These results suggest that the BET surfaces depended on the pyrolysis temperature because surface area increased with rising pyrolysis temperature. In the current study, the adsorption of Cu^{2+} ions improved at higher pyrolysis temperatures of 500 to 800 °C, which may have been due to the increase in the BET surface area.

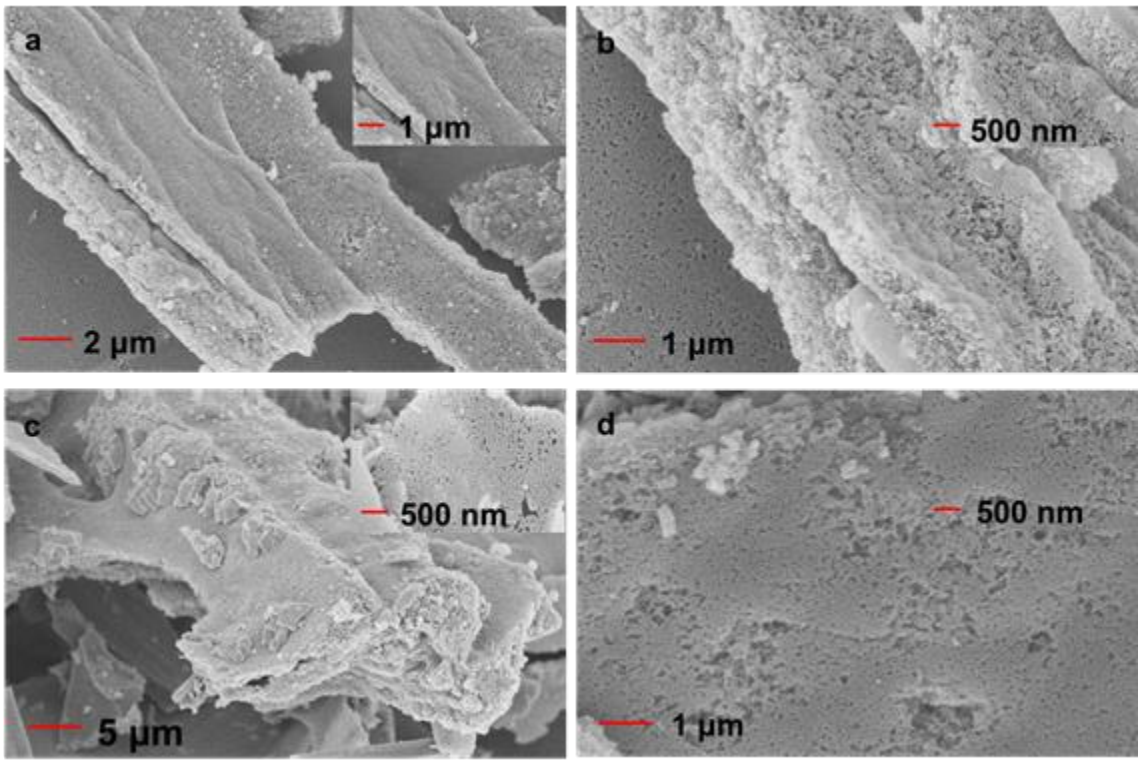

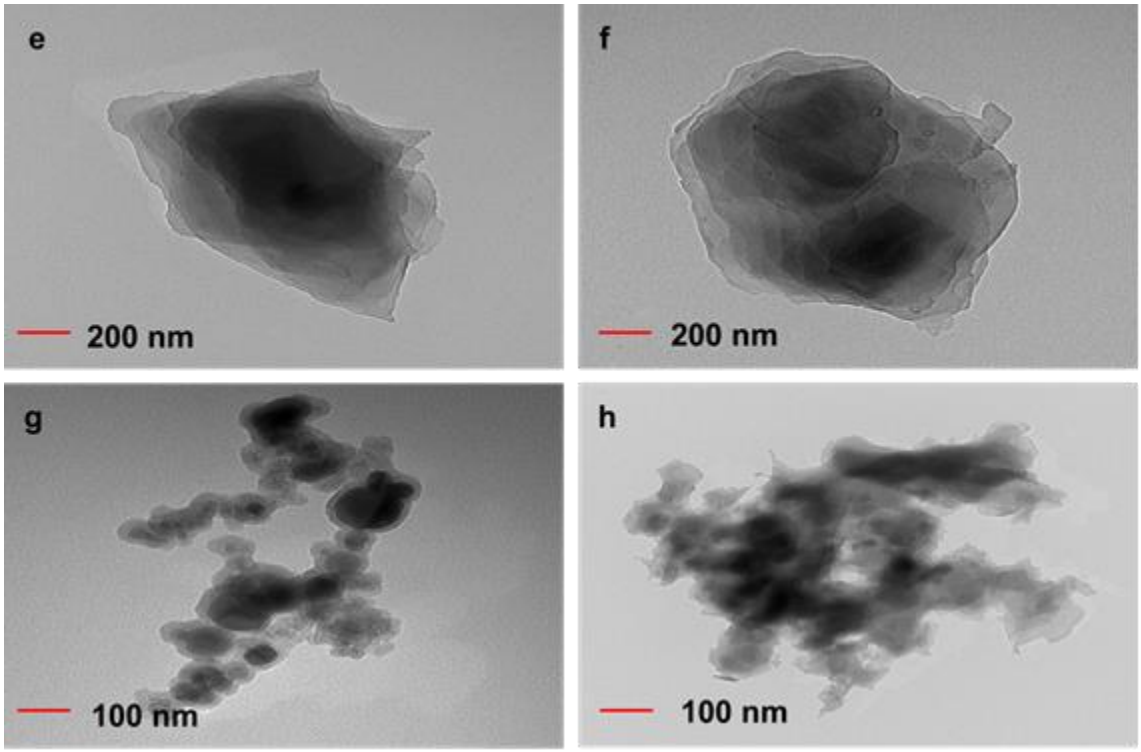

Fig. 1. SEM (a through d) and TEM (e through h) images of the biochars

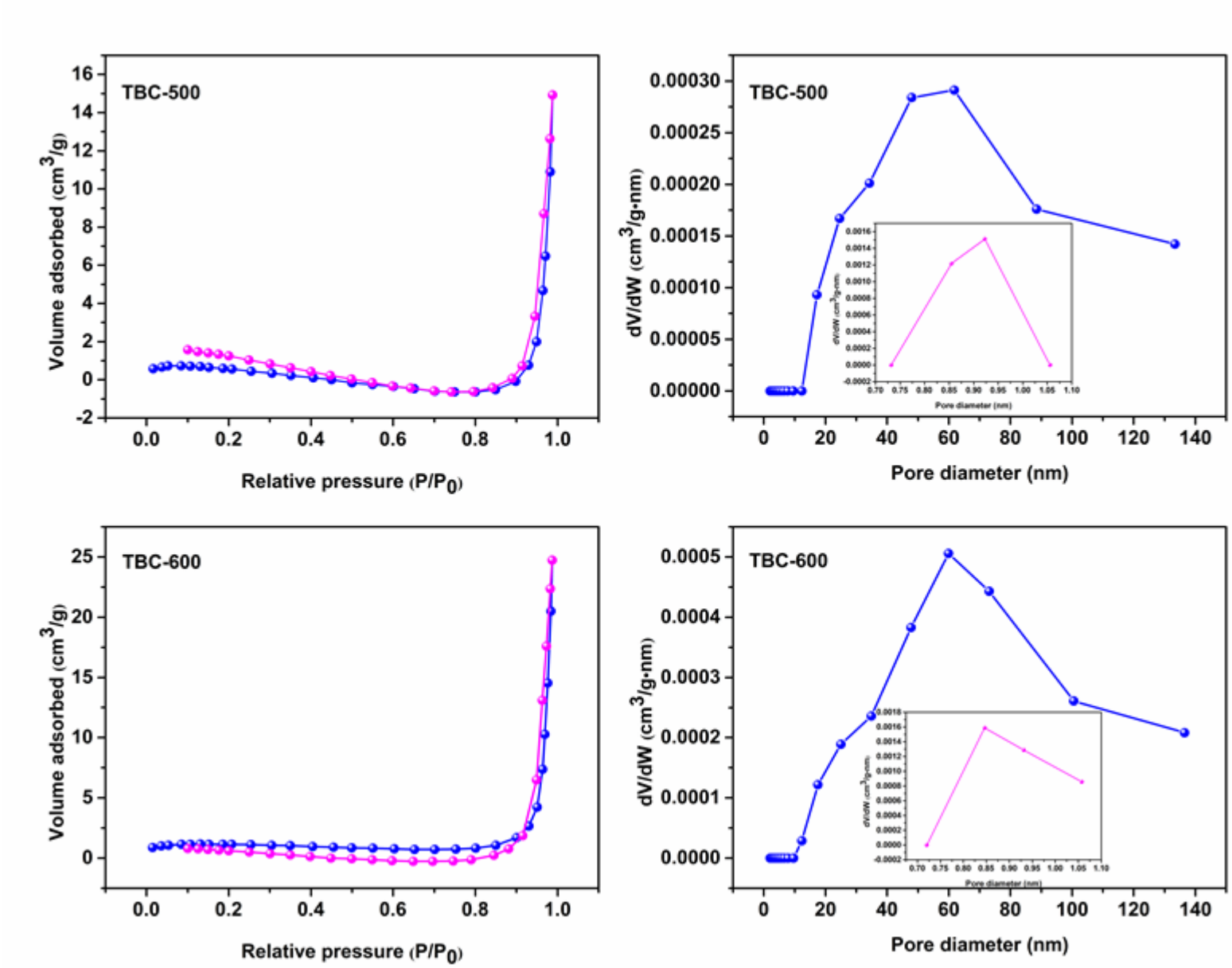
TBC-500
Volume adsorbed (cm3/g)
Relative pressure (P/P0)
TBC-500
dV/dW (cm3/g·nm)
Pore diameter (nm)
TBC-600
Volume adsorbed (cm3/g)
Relative pressure (P/P0)
TBC-600
dV/dW (cm3/g·nm)
Pore diameter (nm)

1

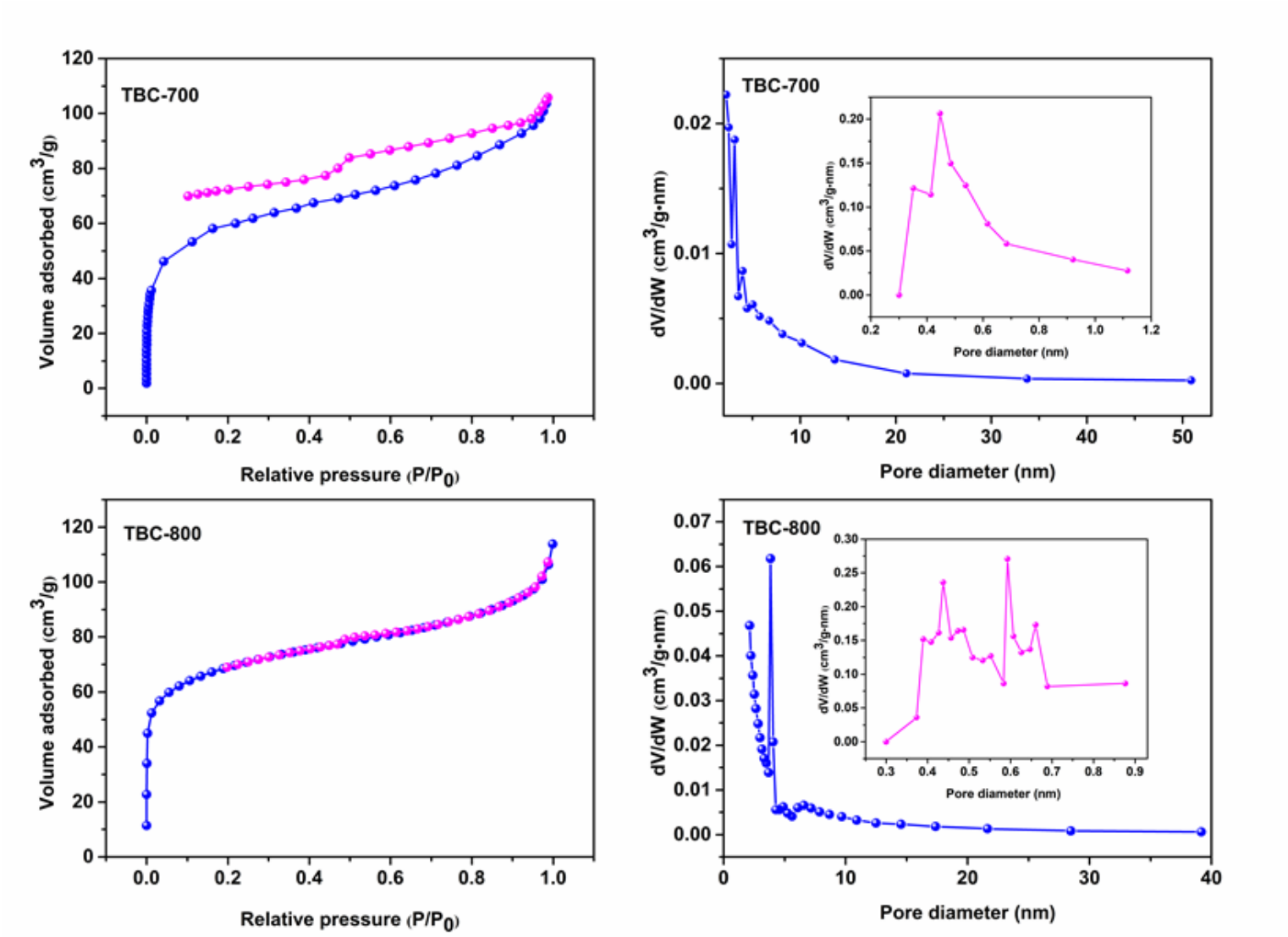

Fig. 2. Nitrogen adsorption-desorption isotherms and pore size distribution of the biochars

The elemental compositions of the biochars are listed in Table 1. The carbon contents of TBC-500, TBC-600, TBC-700, and TBC-800 were 65.6, 67.4, 68.8, and 76.2%, respectively. Carbon content increased, whereas hydrogen, oxygen, and nitrogen contents decreased, resulting in a decrease in the H/C, O/C, N/C, and (N+O)/C molar ratios (due to high carbonization and removal of polar functional groups). The O/C ratio was lower, suggesting that the TBC surface became less hydrophilic at higher temperatures. The polarity index indicator ((N+O)/C) decreased, which was attributed to the formation of aromatic structures by higher carbonization of the TBC and removal of polar surface functional groups. The N content of TBC only depended on feedstock characteristics and not on pyrolysis temperature.

The physicochemical characteristics of the four biochars are shown in Table 1. The pH of the biochars increased slowly from 10.3 to 10.9 when the pyrolysis temperature was increased from 500 to 800 °C. Other studies have reported that a high biochar pH was obtained with a higher pyrolysis temperature (Chen *et al.* 2011). Cellulose and hemicellulose decompose at 200 to 300 °C to produce organic acids and phenolic compounds that decrease the pH of biochars (Rangabhashiyam and Balasubramanian 2019). Alkali salts are released from the pyrolytic structure when the pyrolysis temperature and pH of the biochar are higher (Goswami *et al.* 2016).

Table 1. Physicochemical Characteristics of the Four Biochars

Biochar	TBC-800	TBC-700	TBC-600	TBC-500
pH	10.86	10.45	10.30	10.26
C (%)	76.25 ± 0.05	68.83 ± 0.03	67.37 ± 0.05	65.59 ± 0.04
N (%)	0.58 ± 0.002	0.35 ± 0.003	0.38 ± 0.01	0.39 ± 0.005
H (%)	1.40 ± 0.07	1.78 ± 0.03	2.26 ± 0.01	3.19 ± 0.02
O (%)	2.19 ± 0.15	11.84 ± 0.14	13.24 ± 0.09	15.37 ± 0.11
H/C	0.018 ± 0.01	0.025 ± 0.007	0.033 ± 0.006	0.049 ± 0.01
N/C	$7.6 \pm 0.01 \times 10^{-3}$	$5.1 \pm 0.01 \times 10^{-3}$	$5.6 \pm 0.01 \times 10^{-3}$	$5.9 \pm 0.01 \times 10^{-3}$
O/C	0.03 ± 0.004	0.17 ± 0.005	0.19 ± 0.008	0.23 ± 0.005
(N+O)/C	0.04 ± 0.003	0.18 ± 0.009	0.20 ± 0.003	0.24 ± 0.002
Ca (mg/kg)	$8.40 \pm 0.1 \times 10^4$	$8.36 \pm 0.1 \times 10^4$	$8.04 \pm 0.3 \times 10^4$	$3.85 \pm 0.4 \times 10^4$
Mg (mg/kg)	$3.52 \pm 0.1 \times 10^3$	$3.38 \pm 0.1 \times 10^3$	$3.04 \pm 0.1 \times 10^3$	$2.67 \pm 0.1 \times 10^3$
Fe (mg/kg)	$3.37 \pm 0.2 \times 10^2$	$3.13 \pm 0.4 \times 10^2$	$2.65 \pm 0.1 \times 10^2$	$1.52 \pm 0.1 \times 10^2$
K (mg/kg)	$1.15 \pm 0.2 \times 10^4$	$1.06 \pm 0.1 \times 10^4$	$1.09 \pm 0.1 \times 10^4$	$7.79 \pm 0.1 \times 10^3$
Cu (mg/kg)	3.65 ± 0.03 × 10	3.61± 0.05 × 10	2.97 ± 0.1 × 10	3.55 ± 0.03 × 10
Mn (mg/kg)	4.77 ± 0.1 × 10	4.56 ± 0.3 × 10	4.52 ± 0.2 × 10	3.33 ± 0.3 × 10
Zn (mg/kg)	2.57 ± 0.04 × 10	6.09 ± 0.08 × 10	8.45 ± 0.05 × 10	6.54 ± 0.1 × 10
SBET (m^2/g)	236.41	202.27	3.82	1.81
Ash (%)	19.58 ± 0.05	17.20 ± 0.06	16.75 ±0.03	15.46 ± 0.05

The ash contents of TBC-500, TBC-600, TBC-700, and TBC-800 were 15.5, 16.8, 17.2, and 19.6%, respectively. Ash content depends on the pyrolysis temperature. The mineral elemental contents of the biochars were also investigated with the elements of interest being Ca, Mg, Fe, K, Cu, Mn, and Zn. Calcium and potassium contents were significantly higher than the other mineral elements. The abundance of Ca was attributed to low organic matter. Furthermore, the abundant mineral elements provided many ion exchange sites between Cu and the cations (Ca^{2+}, K^+, and Mg^{2+}) during adsorption of Cu^{2+} ions which allowed the adsorption to take place at a higher rate. The Cu, Mn, and Zn contents of all biochars were lower than the other mineral elements; thus, they were considered negligible with respect to the adsorption experiments.

FTIR Analysis

The surface functional groups on the TBC from different pyrolysis conditions were detected by FT-IR. Figure 6a shows that the TBC had a wide band at about 3,447 cm^{-1}, which was assigned to the O-H vibrations of the hydroxyl groups (Aran *et al.* 2016; Vyavahare *et al.* 2018). The absorption peak at 2,921 cm^{-1} was attributable to the -CH_2 groups of aliphatic components (Aran *et al.* 2016). The peak at 1,579 cm^{-1} corresponded to the antisymmetric stretching vibrations of -COOH (Tong *et al.* 2011). The four types of biochars had a similar particularly intense infrared absorption band at 1,433 cm^{-1}, which was attributed to in-plane bending of the carbonyl (-COH) groups. (Yuan *et al.* 2011). The intensity of the peak at 1,433 cm^{-1} increased with increasing pyrolysis temperature, suggesting the presence of carbonate in the biochars (Aran *et al.* 2016). The peak at 1,700 cm^{-1} was attributed to C=O bonds from cellulose and lignin in TBC-500 (Petrovic *et al.* 2016). The number of functional groups on the surfaces of the biochars decreased during pyrolysis under increasing temperature and differed distinctly from those on the feedstocks. A peak at 1,262 cm^{-1} was assigned to phenolic -OH stretching (Chen *et al.* 2011; Ding *et al.* 2016). Bands at 874, 812, and 751 cm^{-1} corresponded to aromatic C-H banding (Aran *et al.* 2016; Ding *et al.* 2016). The FT-IR spectral results indicated fewer polar functional groups on the TBC, which was consistent with the elemental analysis.

X-ray Diffraction Analysis

The XRD spectra of the biochars produced at different pyrolysis temperatures are shown in Fig. 3. The cellulose crystalline structure was totally destroyed due to the high temperature. All biochars in the present study revealed a similar graphitic and inorganic structure. The diffraction peaks between 15° and 30° 2θ in the biochars were attributed to aromatic carbons. The peak at 29.50° 2θ provided evidence for the presence of calcite ($CaCO_3$) in all of the biochars (Yuan *et al.* 2011). The FT-IR spectral and elemental analyses were further supported by the XRD pattern. The peak intensity at 29.5° 2θ increased as pyrolysis temperature was increased from 500 to 800 °C, indicating that the calcite content of the biochar increased with increasing pyrolysis temperature which was consistent with the change in peak intensity at 1,433 cm^{-1} in the FT-IR and elemental analyses. The presence of calcite was consistent with the alkalinity of the biochars. Moreover, the intense sharp peak at 29.5° 2θ suggested that the calcite was well crystallized. The peaks at 28.5° and 40.9° 2θ provided evidence for the presence of KCl in the biochars (Wang *et al.* 2016). A few crystalline substances, such as magnesium calcite ($MgCO_3$), calcium oxalate (CaC_2O_4), and dolomite (Ca/Mg $(CO_3)_2$), appeared in the biochars. The XRD analysis was consistent with the elemental analysis.

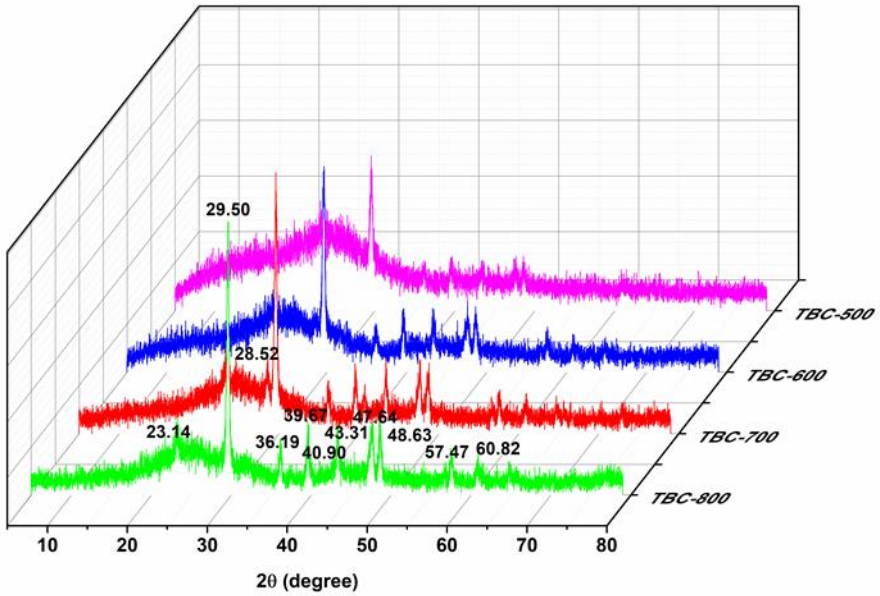

Fig. 3. The X-ray diffraction spectra for the biochars produced from *T. papyriferum* at different pyrolysis temperatures

Effect of pH on the Adsorption of Cu^{2+} Ions

The initial pH of a solution is an important factor in adsorption. The pH was selected in the range of 2.0 to 5.0 to avoid formation of a $Cu(OH)_2$ precipitate. The results indicated that the adsorption capacity of all four biochars increased as the pH was increased from 2.0 to 5.0 (Fig. 4g), indicating a low adsorption capacity at pH 2.0. These results can be explained by the competition of a large number of hydrogen and Cu^{2+} ions for adsorption sites on the biochars at a lower pH (Chen *et al.* 2011). Hence, all subsequent experiments in this study were carried out at the optimum initial pH value of 5.0 where maximum adsorption was obtained.

Adsorption Kinetics

The effect of contact time on the adsorption capacity of the biochars is shown in Fig. 4a. All experiments used 100 mg/L Cu^{2+} under constant stirring at 180 rpm and temperature set to 30 °C. Sorption was rapid during the first 20 min and reached equilibrium within 60 min for all biochars, showing efficient adsorption. This rapid adsorption rate at the initial stage of adsorption was attributed to the high surface area and the presence of a large number of available adsorption sites on the biochars at this stage. The rate of adsorption was faster than other materials in the biochars, as reported in previous studies (Chen *et al.* 2011; Pellera *et al.* 2012; Kılıç *et al.* 2013). The rate of decreased adsorption may be due to the progressive saturation of these active sites (Pellera *et al*. 2012). A different adsorption equilibrium time suggested that pyrolysis temperature played an important role in controlling the adsorption kinetics.

In this study, two adsorption kinetic models were studied to identify the mechanism controlling the adsorption process of Cu^{2+} ions on the biochars. The pseudo-first-order and pseudo-second-order kinetics models were analyzed in this study (Xiao *et al.* 2017).

The equation for the pseudo-first-order kinetics model can be expressed as:

$$(1/Q_t) = (K_1/(Q_e t)) + (1/Q_e) \quad (2)$$

The equation for the pseudo-second-order kinetics model is,

$$(t/Q_t) = (1/(K_2 Q_e^2)) + (t/Q_e) \quad (3)$$

where Q_e and Q_t (mg/g) are the amount of Cu^{2+} ions adsorbed at equilibrium and at time t (min), K_1 (min^{-1}) represents the pseudo-first-order rate constant, and K_2 ($g \cdot mg^{-1} \cdot min^{-1}$) represents the pseudo-second-order adsorption rate constant.

The linear fitting results of the pseudo-first-order and pseudo-second-order kinetic models are displayed in Fig. 4 (c and d), and the adsorption kinetics parameters are summarized in Table 2. High coefficients of determination ($R^2 > 0.99$) were obtained for all biochars with the pseudo-second-order model. Moreover, the equilibrium adsorption capacities calculated by the pseudo-second-order model were consistent with the experimental results.

Table 2. Adsorption Kinetics Parameters for the Adsorption of Cu^{2+} Ions (100 mg/L) on the Biochars

Biochar	Pseudo-first-order			Pseudo-second-order		
	Q_e (mg/g)	K_1 (min^{-1})	R^2	Q_e (mg/g)	K_2($g \cdot mg^{-1} \cdot min^{-1}$)	R^2
TBC-800	40.7664	6.0881	0.9705	39.6983	0.0052	0.9992
TBC-700	39.8565	3.6242	0.9133	39.0472	0.0097	0.9991
TBC-600	43.2152	11.6499	0.9771	39.9202	0.0033	0.9975
TBC-500	31.9591	14.0866	0.9546	28.3527	0.0044	0.9958

Adsorption Isotherms of Cu^{2+} Ions on the Biochar Fractions

The adsorption process was carried out in the range of 25 to 1,000 mg/L at 30 °C for 24 h (180 rpm) to explore the effect of initial ion concentration on adsorption. The effect of initial Cu^{2+} ion concentration on biochar adsorption is shown in Fig. 4b. The adsorption capacity increased with an increase in the initial Cu^{2+} ion concentrations at an initial Cu^{2+} concentration below 400 mg/L, which may have been due to the high initial concentration providing a higher driving force for Cu^{2+} ions to overcome mass transfer resistance in solution (Zhou *et al.* 2017). The adsorption capacity then slowly changed as the initial Cu^{2+} ion concentration increased due to saturation of the available surface active sites on the biochars. The adsorption results indicate that pyrolysis temperature played an important role in adsorption capacity. The difference in the adsorption capacities of the four kinds of biochars may be due to different physicochemical contents (Ca, Mg, and K) and BET surface areas. The adsorption capacities of the biochars derived from different temperatures were subjected to the order of TBC-800 (182 mg/g) > TBC-700 (142 mg/g) > TBC-600 (77 mg/g) > TBC-500 (50 mg/g). Thus, higher pyrolysis temperatures were favorable to produce biochars with a higher adsorption capacity of Cu^{2+} ions. Overall, TBC-800 showed the fastest kinetics and the highest capacity for Cu^{2+} ions, and it was the best sorbent among the tested biochars.

The Langmuir and Freundlich isothermal models were used to analyze the results of the equilibrium isotherms and to better understand the adsorption mechanism of Cu^{2+} ions on the biochars (Kim *et al.* 2016; Zhou *et al.* 2017). The Langmuir and Freundlich models were deduced from different theoretical assumptions. The Langmuir isotherm model is based on the assumption that monolayer adsorption and adsorption occur at

specific homogeneous sites within the adsorbent. The Langmuir (Eq. 4) and Freundlich (Eq. 5) adsorption isotherm models are expressed as follows:

$$(C_e/Q_e) = (C_e/Q_{max}) + (1/(K_L Q_{max})) \quad (4)$$

$$\log Q_e = \log K_F + (1/n)(\log C_e) \quad (5)$$

where Q_e is the equilibrium Cu^{2+} ion adsorption capacity (mg/g), Q_{max} is the maximum adsorption capacity (mg/g), K_L is the Langmuir constant (L/mg), K_F is the Freundlich constant (mg/g), C_e is the equilibrium concentrations of Cu^{2+} ions (mg/L), and $1/n$ is adsorption intensity (Units).

Figure 4 (e and f) presents the curve fitting for the adsorption results using the Langmuir and Freundlich models; the calculated parameters are shown in Table 3. According to the R^2 values of the results presented in Table 3, the Langmuir adsorption model provided the best fit for the experimental data of all biochars with $R^2 > 0.99$. The model suggested the formation of a monolayer of metal ions on the surface of the biochars. The maximum adsorption capacities of the biochars were 181 mg/g (TBC-800), 132 mg/g (TBC-700), 78 mg/g (TBC-600), and 57 mg/g (TBC-500).

Table 3. Adsorption Isotherm Parameters for the Adsorption Cu^{2+} Ions on the Biochars

Biochar	Langmuir			Freundlich		
	Q_{max} (mg/g)	K_L (L/mg)	R_L^2	K_F (mg/g)	n	R_F^2
TBC-800	181.1594	0.2395	0.9990	47.8784	4.4545	0.7323
TBC-700	132.4503	0.5491	0.9997	52.9529	5.7594	0.7390
TBC-600	78.3085	0.2054	0.9997	16.8019	3.1861	0.7835
TBC-500	57.3724	0.0166	0.9989	3.2252	2.0471	0.9101

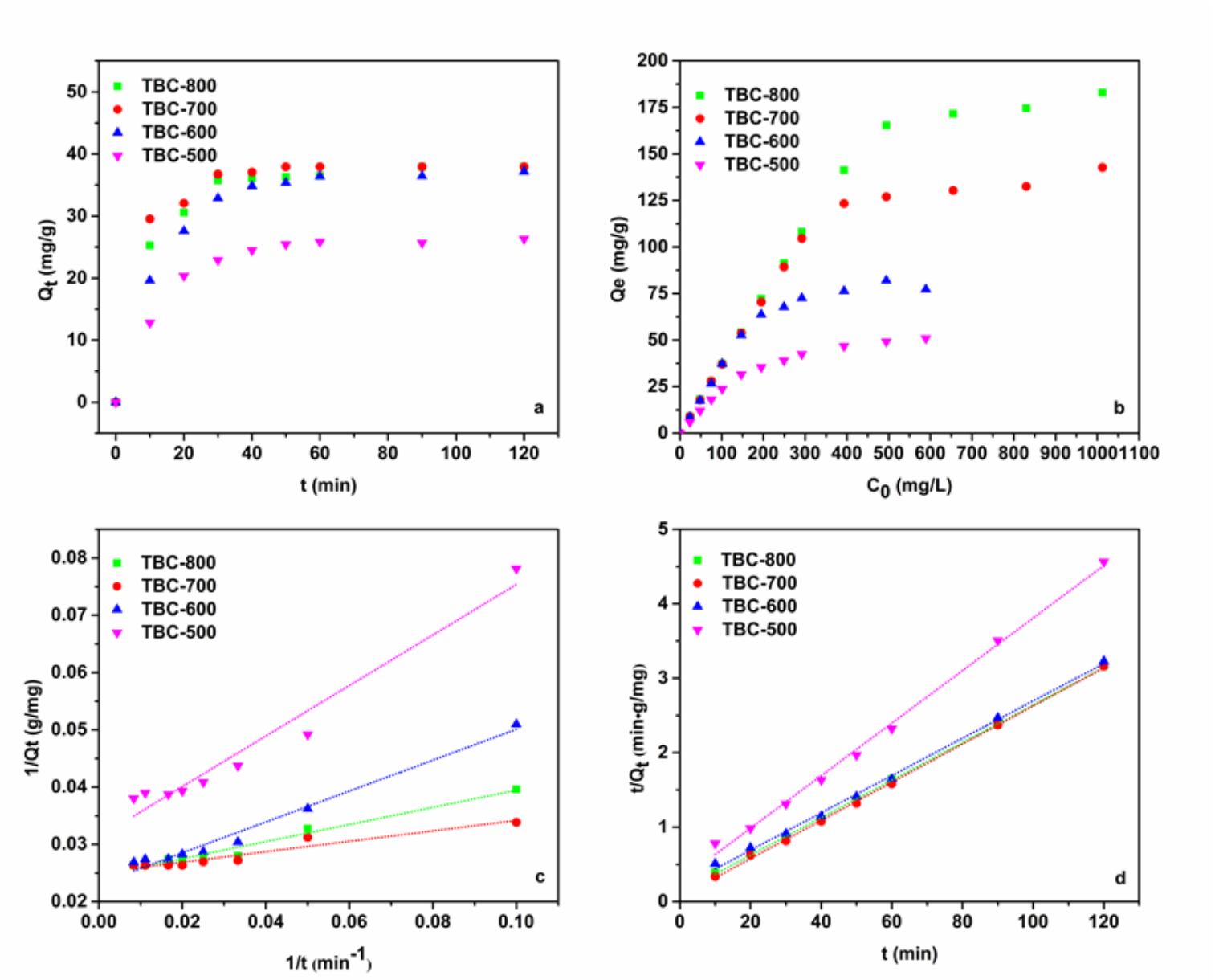
TBC-800
TBC-700
TBC-600
TBC-500
Qt (mg/g)
t (min)
a
Qe (mg/g)
C0 (mg/L)
b
1/Qt (g/mg)
1/t (min-1)
c
t/Qt (min-g/mg)
t (min)
d

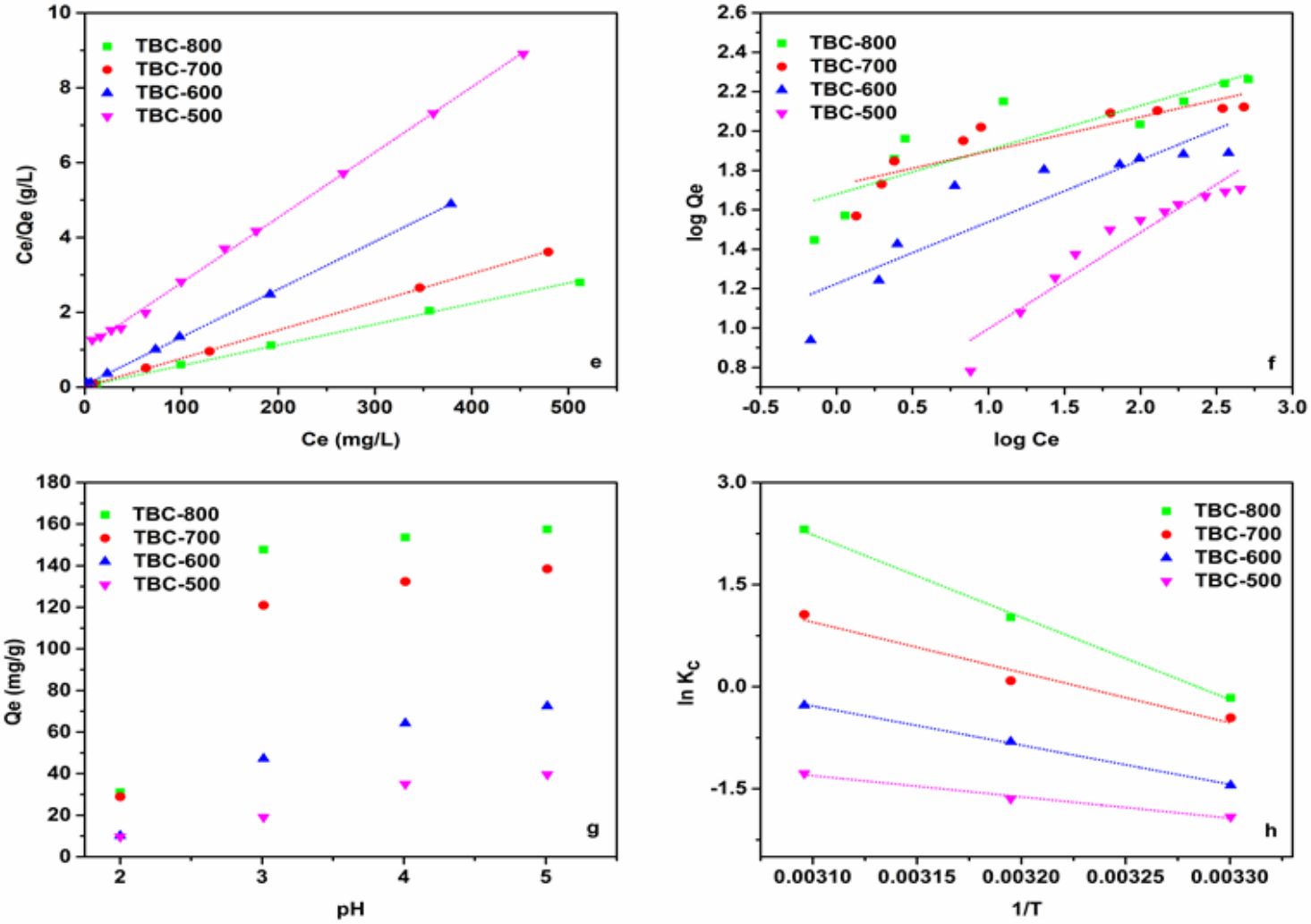

Fig. 4. The effect of contact time (a), initial Cu^{2+} ions concentration (b), and initial solution pH (g) on TBC adsorption of Cu^{2+} ions; Adsorption kinetics of Cu^{2+} ions adsorption by linear plots of pseudo-first-order (c) and pseudo-second-order (d) rate equations on the biochars; Adsorption isotherms of Langmuir (e) and Freundlich (f) models; Van't Hoff plot (h) for the adsorption of Cu^{2+} ions on the biochars

The adsorption capacities of the biochars were compared with those reported previously in Table 4. The maximum adsorption capacity of TBC (181 mg/g) was higher than that of the biochars produced from different biomasses including rice (44.47 mg/g), hardwood (12.5 mg/g), earthworm manure (36.6 mg/g), rice husk (5.6 mg/g), sugarcane (40.5 mg/g), peanut straw (88.9 mg/g), *Undaria pinnatifida* (125.8 mg/g), and *Enteromorpha compressa* (137 mg/g). Better adsorption capacity of TBC for the removal of Cu^{2+} was due to more active sites and higher mineral elemental contents than other adsorbents. Therefore, this study showed that TBC was a good adsorbent for removing Cu^{2+} ions from aqueous solution.

Table 4. Comparison of Adsorption Capacities of Biochars Reported Herein Toward Heavy Metal Ions with Those Reported in the Literature

Adsorbent (Biochar)	Adsorption of Cu^{2+} Ions Capacity (mg/g)	References
Rice	44.5	(Aran *et al.* 2016)
Hardwood	12.5	(Chen *et al.* 2011)
Earthworm manure	36.6	(Wang *et al.* 2017)
Rice husk	5.6	(Guo *et al.* 2014)
Cattle manure	44.5	(Idrees *et al.* 2018)
Sugarcane	40.5	(Hass and Lima, 2018)
Peanut straw	88.9	(Tong *et al.* 2011)
Undaria pinnatifida	125.8	(Cho *et al.* 2013)
Enteromorpha compressa	137	(Kim *et al.* 2016)
Tetrapanax papyriferum	181.2	This work

Adsorption Thermodynamics

The thermodynamics of adsorption of the biochars were investigated in the temperature range of 303 to 323K. The standard free energy change ($\Delta G°$), standard enthalpy change ($\Delta H°$), and standard entropy ($\Delta S°$) were calculated from the van't Hoff equation (He *et al.* 2017),

$$\Delta G° = -RT\ln K_c \quad (6)$$

$$\ln K_c = (\Delta S°/R) - (\Delta H°/RT) \quad (7)$$

$$K_c = Q_e/C_e \quad (8)$$

where R, T, and K_c represent the gas constant (8.314 J mol^{-1} K^{-1}), the temperature in Kelvin, and the adsorption equilibrium constant, respectively. Q_e (mg/g) is the amount of absorbed biochar per unit mass of adsorbent at equilibrium, and C_e (mg/L) is the equilibrium Cu^{2+} ion concentration.

The adsorption capacity increased as temperature increased, indicating that adsorption is an endothermic process. The increase in temperature might provide the Cu^{2+} ions sufficient energy to overcome the diffuse layer and adsorb onto the interior structure of the biochars (Chen *et al.* 2011). The thermodynamic parameters are shown in Table 5. Negative values of ΔG^o indicate that the process was spontaneous and feasible for Cu^{2+} ion adsorption. The TBC-800 and TBC-700 $\Delta G°$ values ranged from positive to negative for the adsorption of Cu^{2+} ions, indicating less spontaneous Cu^{2+} ion adsorption at lower temperatures but improved activity at higher temperatures. Moreover, the $\Delta G°$ values decreased with the increase in temperature, indicating decreased sorption at high

temperatures. The positive value of $\Delta H°$ indicated that all Cu^{2+} ion adsorption processes on the biochars are endothermic and that higher temperatures are preferred for higher sorption. This is consistent with the observed trend in Cu^{2+} ion adsorption capacity. The positive $\Delta S°$ value indicated that randomness increased at the solid/solution interface during the adsorption process.

Table 5. Adsorption Thermodynamics Parameters for the Adsorption of Cu^{2+} on the Biochars

Biochar	ΔG° (KJ/mol)			ΔH° (KJ/mol)	ΔS° (J/mol/K)	R^2
	303 K	313 K	323 K			
TBC-800	0.4887	-2.8165	-6.1217	100.6366	330.5210	0.9963
TBC-700	1.3430	-0.6427	-2.6284	61.5101	198.5711	0.9359
TBC-600	3.6215	2.1606	0.6998	47.8843	146.0821	0.9979
TBC-500	4.8706	4.1737	3.4768	25.9872	69.6917	0.9754

Reutilization Efficiency of TBC

Testing the reuse of an adsorbent is critical for evaluating the reusability and sustainability of the adsorbent. Batch experiments were carried out to demonstrate the efficiency of TBC for adsorbing Cu^{2+} ions over four repeated cycles. Figure 5 shows that 99.99% sorption of Cu^{2+} was observed on the TBC during the first cycle; however, sorption capacity declined to 80.4% during the fourth cycle. The overall observations showed that the TBC has the potential to be reutilized for consecutive sorption of Cu^{2+} ions.

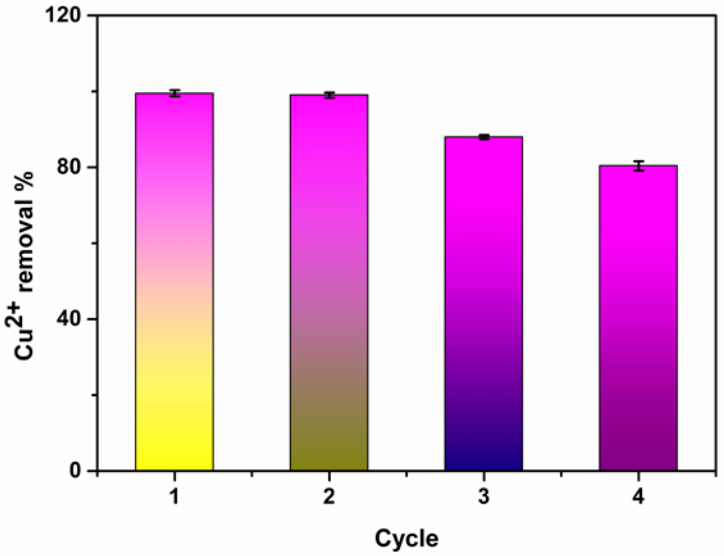

Fig. 5. Recyclability of TBC-700 for the adsorption of Cu^{2+} ions

Adsorption Mechanism

The FT-IR and XPS spectra were further employed to elucidate the Cu^{2+} ion adsorption mechanisms shown in Fig. 6. Several differences in the FT-IR spectra were observed for the TBC after Cu^{2+} ion adsorption. The typical bands for calcite in the TBC at about 1,440 and 875 cm^{-1} was decrease in intensity after the Cu^{2+} ions were adsorbed. This observation was in agreement with the XPS results of the elemental analysis. The

XPS results confirmed that the atomic percentage of Cu increased, whereas that of Ca decreased after sorption, which confirmed the proposed precipitation and ion exchange mechanism. The bands assigned to -OH stretching vibrations at 3,441 cm^{-1} shifted to 3,418 cm^{-1}, and the corresponding peaks of anti-symmetric stretching vibrations of the -COOH groups at 1,605 cm^{-1} for TBC-500 were shifted to 1,587 cm^{-1}. These results are consistent with a hypothesis that the -COOH and phenolic hydroxyl groups reacted with Cu (II) to form surface complexes. The band at about 1,083 cm^{-1} was shifted towards 1,068 and 1,116 cm^{-1} due to a reduction of Cu^{2+} ions and formation of cuprocyanide from C-N (Batool *et al*. 2017). The peak at 1,687 cm^{-1}, which was ascribed to C=C stretching vibrations in TBC-500, disappeared after Cu^{2+} ion adsorption, indicating that π-π interactions are involved in Cu^{2+} ion adsorption (Dai *et al*. 2018). The appearance of new peaks at 601 cm^{-1} and 933 eV in the Cu-laden TBC confirmed the formation of stable CuO (Batool *et al*. 2017).

TBC exhibited low surface area and higher adsorption capacity; thus, the contribution of pore filling was negligible for Cu^{2+} adsorption. So other adsorption mechanisms, including intraparticle diffusion, precipitation, complexation, and π-π interactions might be responsible for Cu^{2+} removal. TBC contains a significant amount of ash (15 to 20%). Except for C, H, and N, other abundant mineral elements in the TCB included Ca, Mg, Zn, Cu, Fe, and Mn and Ca was most abundant. According to the XRD and FTIR analysis, the abundant of carbonates ($CaCO_3$) in TBC, a lot of research indicating heavy metals was adsorbed through the precipitation mechanism (Xu *et al*. 2017; Zhou *et al*. 2017). The bands ascribed to the calcite in the TBC at 1432 cm^{-1} was decreased after Cu^{2+} ion adsorption, which was consistent with the intensities of the peaks about Ca_{2p} at 348 eV in XPS spectra. These results suggested that the precipitation interaction was related to carbonate in the TBC. The XPS results confirmed that the atomic percentage of the Cu was increased, whereas the Ca was decreased after sorption, which was confirming the proposed precipitation and ion exchange mechanism. The new peaks at 601 cm^{-1} and 933 eV in the Cu-laden TBC confirmed the formation of stable CuO (Idrees *et al.* 2018). Except the precipitation mechanism, the FTIR analysis has proved the surface complexation and π-π interactions mechanism. These results indicate that the -COOH, -OH and phenolic hydroxyl groups reacted with Cu (II) to form surface complexes. In summary, precipitation, surface complexation and π-π interactions were involved in the extraordinarily adsorption of Cu^{2+} onto TBC.

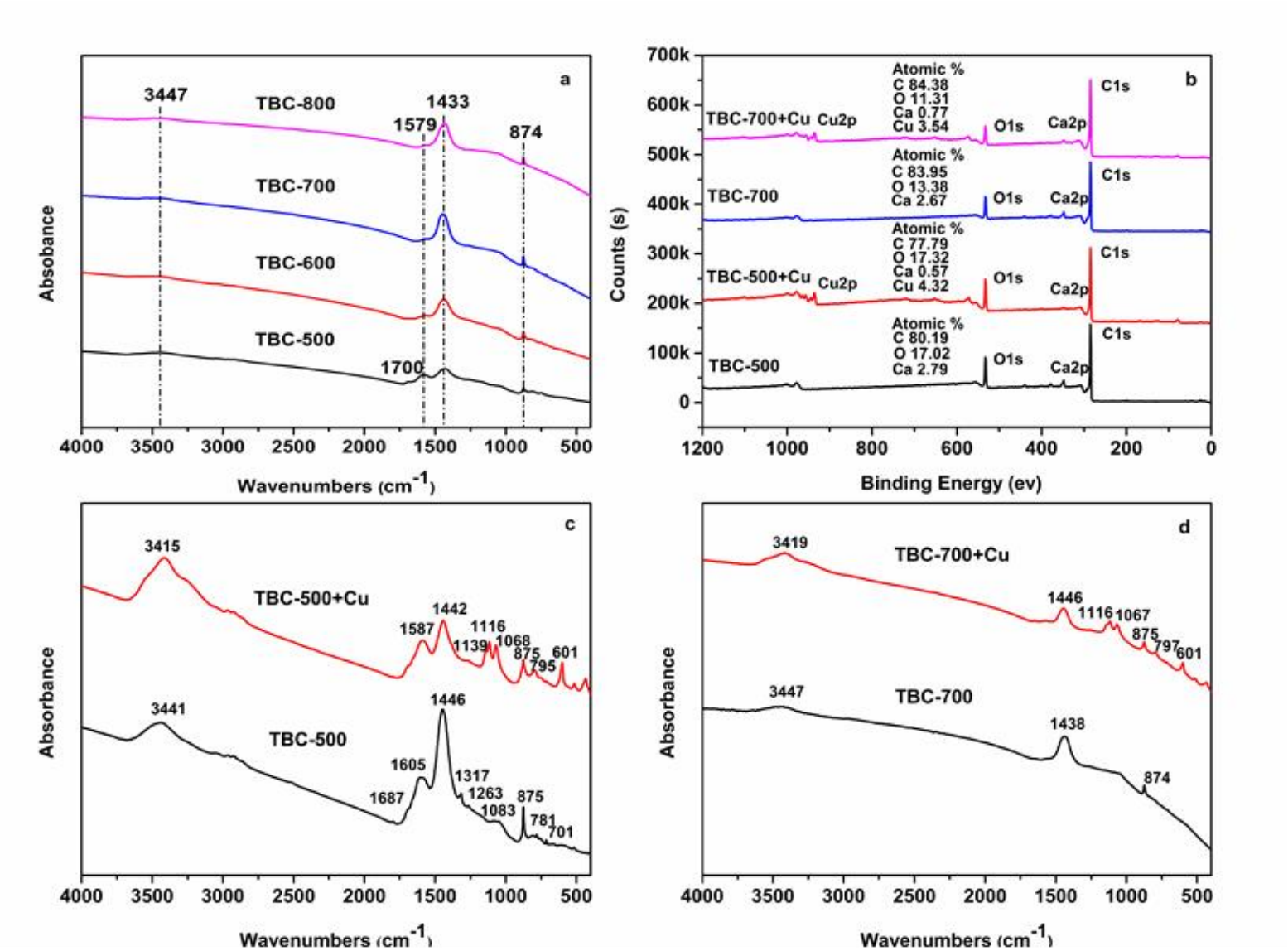

Fig. 6. FTIR spectra of the biochars (a), X-ray photoelectron spectra (b), FTIR spectra of TBC-500 (c), and TBC-700 (d) before and after Cu^{2+} ions sorption

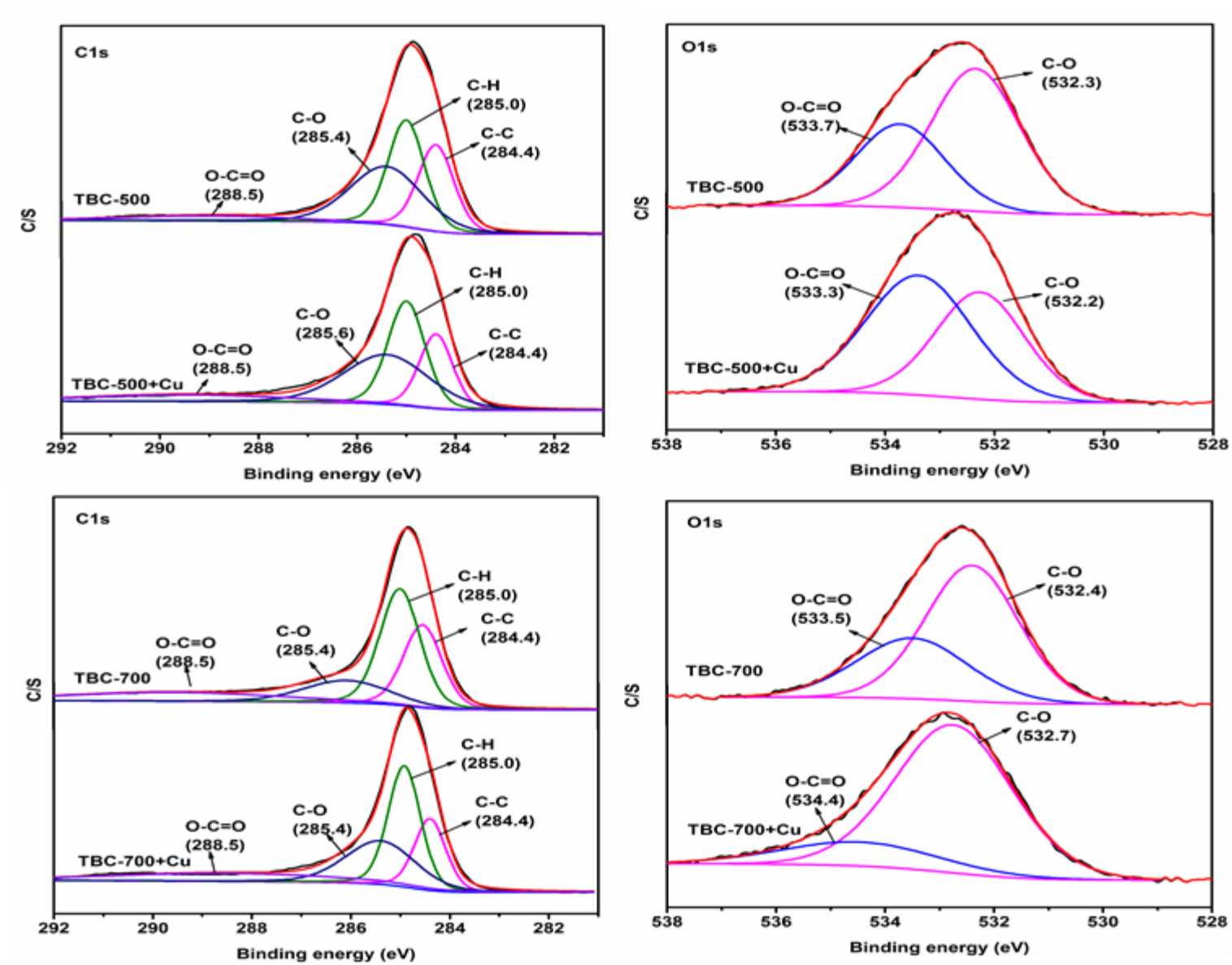

Fig. 7. High-resolution XPS spectra of C_{1s} and O_{1s} in TBC-500 and TBC-700 before and after Cu^{2+} ions sorption

The high-resolution C_{1s} and O_{1s} for TBC were deconvoluted into different peaks to understand the stable chemical state after Cu^{2+} ion adsorption in Fig. 7. The well-fitted deconvoluted peak for C_{1s} at 284.4 ± 0.1 eV was assigned to C-C, 285.0 ± 0.1 eV was assigned to C-H, 285.4 ± 0.1 eV was assigned to C-O, and 288.5 ± 0.1 eV was assigned to O-C=O. The binding energies of O_{1s} at 532.3 eV and 533.4 eV were assigned to C-O and O-C=C, respectively. The C_{1s} and O_{1s} deconvoluted peaks in the XPS spectrum were consistent with the FT-IR results. According to the percentage of atoms in XPS, the increase in pyrolysis temperature changed the surface contents of C and O, but not their surface species. In summary, precipitation, ion exchange, C-π interactions, and complexation were involved in adsorption of Cu^{2+} ions onto TBC.

CONCLUSIONS

1. In this study, biochar (TBC) was derived from *Tetrapanax papyriferum* petiole by high temperature pyrolysis, and the influence of temperature (500 °C to 800 °C) on biochar characteristics was investigated.
2. The surface area, mineral elements, and adsorption capacity of the resulting biochars were significantly affected by pyrolysis temperature.
3. The TBC-800 was the most effective for sorption of Cu^{2+} ions with a total of 182 mg/g.
4. The adsorption capacity to remove Cu^{2+} ions remained high even after four adsorption cycles.
5. The adsorption process of Cu^{2+} by TBC was found to be dominated by precipitation, complexation, and π-π interactions.

ACKNOWLEDGMENTS

This work was supported by the Anhui Provincial Natural Science Foundation of China (1808085MC68), the Innovation Fund of Postgraduate of Anhui Agricultural University (2018yjs-16), the Anhui Provincial Training Program of Innovation and Entrepreneurship for Undergraduates (201710364066, XJC2017131 and XJDC2017156), the China Postdoctoral Science Foundation Grant (2016M601996), the Anhui Postdoctoral Science Foundation Grant (2017B157), the National Science and Technology Program of the Thirteenth Five-Year Plan Period (2017YFD0600805-1), and the key research and development project of Anhui Province (1804g07020168).

REFERENCES CITED

Aran, D., Antelo, J., Fiol, S., and Macias, F. (2016). "Influence of feedstock on the copper removal capacity of waste-derived biochars," *Bioresource Technology* 212, 199-206. DOI: 10.1016/j.biortech.2016.04.043

Batool, S., Idrees, M., Hussain, Q., and Kong, J. (2017). "Adsorption of copper (ii) by using derived-farmyard and poultry manure biochars: Efficiency and mechanism,"

Chemical Physics Letters 689, 190-198. DOI: 10.1016/j.cplett.2017.10.016

Chen, X., Chen, G., Chen, L., Chen, Y., Lehmann, J., McBride, M. B., and Hay, A. G. (2011). "Adsorption of copper and zinc by biochars produced from pyrolysis of hardwood and corn straw in aqueous solution," *Bioresource Technology* 102(19), 8877-8884. DOI: 10.1016/j.biortech.2011.06.078

Cho, H. J., Baek, K., Jeon, J. K., Park, S. H., Suh, D. J., and Park, Y.-K. (2013). "Removal characteristics of copper by marine macro-algae-derived chars," *Chemical Engineering Journal* 217(1), 205-211. DOI: 10.1016/j.cej.2012.11.123

Dai, L., Zhu, W., He, L., Tan, F., Zhu, N., Zhou, Q., and Hu, G. (2018). "Calcium-rich biochar from crab shell: An unexpected super adsorbent for dye removal," *Bioresource Technology* 267, 510-516. DOI: 10.1016/j.biortech.2018.07.090

Ding, Z., Wan, Y., Hu, X., Wang, S., Zimmerman, A. R., and Gao, B. (2016). "Sorption of lead and methylene blue onto hickory biochars from different pyrolysis temperatures: Importance of physicochemical properties," *Journal of Industrial and Engineering Chemistry* 37, 261-267. DOI: 10.1016/j.jiec.2016.03.035

Goswami, R., Shim, J., Deka, S., Kumari, D., Kataki, R., and Kumar, M. (2016). "Characterization of cadmium removal from aqueous solution by biochar produced from *Ipomoea fistulosa* at different pyrolytic temperatures," *Ecological Engineering* 97, 444-451. DOI: 10.1016/j.ecoleng.2016.10.007

Guo, Y., Tang, W., Wu, J., Huang, Z., and Dai, J. (2014). "Mechanism of Cu(II) adsorption inhibition on biochar by its aging process," *Journal of Environmental Sciences* 26(10), 2123-2130. DOI: 10.1016/j.jes.2014.08.012

Han, Y., Cao, X., Ouyang, X., Sohi, S. P., and Chen, J. (2016). "Adsorption kinetics of magnetic biochar derived from peanut hull on removal of Cr (VI) from aqueous solution: Effects of production conditions and particle size," *Chemosphere* 145, 336-341. DOI: 10.1016/j.chemosphere.2015.11.050

Hass, A., and Lima, I. M. (2018). "Effect of feed source and pyrolysis conditions on properties and metal sorption by sugarcane biochar," *Environmental Technology & Innovation* 10, 16-26. DOI: 10.1016/j.eti.2018.01.007

He, J., Li, Y., Wang, C., Zhang, K., Lin, D., and Kong, L., Liu, J. (2017). "Rapid adsorption of Pb, Cu and Cd from aqueous solutions by β-cyclodextrin polymers," *Applied Surface Science* 426, 29-39. DOI: 10.1016/j.apsusc.2017.07.103

Ho, J. C., Chen, C. L., and Row L. C. (2005). "Flavonoids and benzene derivatives from the flowers and fruit of *Tetrapanax papyriferus*," *Journal of Nature Products* 68, 1773-1775. DOI: 10.1021/np050185t

Idrees, M., Batool, S., Kalsoom, T., Yasmeen, S., Kalsoom, A., Raina, S., Zhuang, Q., and Kong, J. (2018). "Animal manure-derived biochars produced via fast pyrolysis for the removal of divalent copper from aqueous media," *Journal of Environmental Management* 213, 109-118. DOI: 10.1016/j.jenvman.2018.02.003

Kılıç, M., Kırbıyık, Ç., Çepelioğullar, Ö., and Pütün, A. E. (2013). "Adsorption of heavy metal ions from aqueous solutions by bio-char, a by-product of pyrolysis," *Applied Surface Science* 283, 856-862. DOI: 10.1016/j.apsusc.2013.07.033

Kim, B. S., Lee, H. W., Park, S. H., Baek, K., Jeon, J. K., Cho, H. J., Jung, S. C., Kim, S. C., and Park, Y. K. (2016). "Removal of Cu^{2+} by biochars derived from green macroalgae," *Environmental Science and Pollution Research* 23(2), 985-994. DOI: 10.1007/s11356-015-4368-z

Li, H., Dong, X., da Silva, E. B., de Oliveira, L. M., Chen, Y., and Ma, L. Q. (2017). "Mechanisms of metal sorption by biochars: Biochar characteristics and

modifications," *Chemosphere* 178, 466-478. DOI: 10.1016/j.chemosphere.2017.03.072

Lin, Y., Hong, Y., Song, Q., Zhang, Z., Gao, J., and Tao, T. (2017a). "Highly efficient removal of copper ions from water using poly(acrylic acid)-grafted chitosan adsorbent," *Colloid and Polymer Science* 295(4), 627-635. DOI: 10.1007/s00396-017-4042-8

Lin, Y. C., Wang, H. P., Gohar, F., Ullah, M. H., Zhang, X., Xie, D. F., Fang, H., Huang, J., and Yang, J. X. (2017b). "Preparation and copper ions adsorption properties of thiosemicarbazide chitosan from squid pens," *International Journal of Bioogical Macromolecules* 95, 476-483. DOI: 10.1016/j.ijbiomac.2016.11.085

Mishra, V., Majumder, C. B., and Agarwal, V. K. (2012). "Sorption of Zn(II) ion onto the surface of activated carbon derived from eucalyptus bark saw dust from industrial wastewater: isotherm, kinetics, mechanistic modeling, and thermodynamics," *Desalination &Water Treatment* 46(1-3), 332-351. DOI: 10.1080/19443994.2012.677556

Niu, Y., Li, K., Ying, D., Wang, Y., and Jia, J. (2017). "Novel recyclable adsorbent for the removal of copper(II) and lead(II) from aqueous solution," *Bioresource Technology* 229, 63-68. DOI: 10.1016/j.biortech.2017.01.007

Park, J. H., Ok, Y. S., Kim, S. H., Cho, J. S., Heo, J. S., Delaune, R. D., and Seo, D. C. (2016). "Competitive adsorption of heavy metals onto sesame straw biochar in aqueous solutions," *Chemosphere* 142, 77-83. DOI: 10.1016/j.chemosphere.2015.05.093

Pellera, F. M., Giannis, A., Kalderis, D., Anastasiadou, K., Stegmann, R., Wang, J. Y., and Gidarakos, E. (2012). "Adsorption of Cu(II) ions from aqueous solutions on biochars prepared from agricultural by-products," *Journal of Environmental Management* 96(1), 35-42. DOI: 10.1016/j.jenvman.2011.10.010

Petrovic, J. T., Stojanovic, M. D., Milojkovic, J. V., Petrovic, M. S., Sostaric, T. D., Lausevic, M. D., Mihajlovic, and M. L. (2016). "Alkali modified hydrochar of grape pomace as a perspective adsorbent of Pb^{2+} from aqueous solution," *Journal of Environmental Management* 182, 292-300. DOI: 10.1016/j.jenvman.2016.07.081

Qian, L., Zhang, W., Yan, J., Han, L., Gao, W., Liu, R., and Chen, M. (2016). "Effective removal of heavy metal by biochar colloids under different pyrolysis temperatures," *Bioresource Technology* 206, 217-224. DOI: 10.1016/j.biortech.2016.01.065

Rangabhashiyam, S., and Balasubramanian, P. (2019). "The potential of lignocellulosic biomass precursors for biochar production: Performance, mechanism and wastewater application—A review," *Industrial Crops & Products* 128, 405-423. DOI: 10.1016/j.indcrop.2018.11.041

Ren, C., Ding, X., Li, W., Wu, H., and Yang, H. (2017). "Highly efficient adsorption of heavy metals onto novel magnetic porous composites modified with amino groups," *Journal of Chemical & Engineering Data* 62, 1865-1875. DOI: 10.1021/acs.jced.7b00198

Teodoro, F. S., Adarme, O. F. H., Gil, L. F., and Gurgel, L. V. A. (2017). "Synthesis and application of a new carboxylated cellulose derivative. Part II: Removal of Co^{2+}, Cu^{2+} and Ni^{2+} from bicomponent spiked aqueous solution," *Journal of Colloid Interface Science* 487, 266-280. DOI: 10.1016/j.jcis.2016.10.043

Tong, X. J., Li, J. Y., Yuan, J. H., and Xu, R. K. (2011). "Adsorption of Cu(II) by biochars generated from three crop straws," *Chemical Engineering Journal* 172(2-3), 828-834. DOI: 10.1016/j.cej.2011.06.069

Vyavahare, G. D., Gurav, R. G., Jadhav, P. P., Patil, R. R., Aware, C. B., and Jadhav, J. P. (2018). "Response surface methodology optimization for sorption of malachite green dye on sugarcane bagasse biochar and evaluating the residual dye for phyto and cytogenotoxicity," *Chemosphere* 194, 306-315. DOI: 10.1016/j.chemosphere.2017.11.180

Wang, Y. Y., Lu, H. H., Liu, Y. X., and Yang, S.-M. (2016). "Ammonium citrate-modified biochar: An adsorbent for La(III) ions from aqueous solution," *Colloids and Surfaces A: Physicochemical and Engineering Aspects* 509, 550-563. DOI: 10.1016/j.colsurfa.2016.09.060

Wang, Z., Shen, F., Shen, D., Jiang, Y., and Xiao, R. (2017). "Immobilization of Cu^{2+} and Cd^{2+} by earthworm manure derived biochar in acidic circumstance," *Journal of Environmental Sciences* 53(3), 293-300. DOI: 10.1016/j.jes.2016.05.017

Xiao, C., Liu, X., Mao, S., Zhang, L., and Lu, J. (2017). "Sub-micron-sized polyethylenimine-modified polystyrene/Fe_3O_4 /chitosan magnetic composites for the efficient and recyclable adsorption of Cu(II) ions," *Applied Surface Science* 394, 378-385. DOI: 10.1016/j.apsusc.2016.10.116

Xu, X., Hu, X., Ding, Z., Chen, Y., and Gao, B. (2017). "Waste-art-paper biochar as an effective sorbent for recovery of aqueous Pb(II) into value-added PbO nanoparticles," *Chemical Engineering Journal* 308, 863-871. DOI: 10.1016/j.cej.2016.09.122

Yuan, J. H., Xu, R. K., and Zhang, H. (2011). "The forms of alkalis in the biochar produced from crop residues at different temperatures," *Bioresource Technology* 102(3), 3488-3497. DOI: 10.1016/j.biortech.2010.11.018

Zhang, Q., Li, Y., Yang, Q., Chen, H., Chen, X., Jiao, T., Peng, Q. (2018a). "Distinguished Cr(VI) capture with rapid and superior capability using polydopamine microsphere: Behavior and mechanism," *Journal of Hazardous Materials* 342, 732-740. DOI: 10.1016/j.jhazmat.2017.08.061

Zhang, X., Fu, W., Yin, Y., Chen, Z., Qiu, R., Simonnot, M. O., and Wang, X. (2018b). "Adsorption-reduction removal of Cr(VI) by tobacco petiole pyrolytic biochar: Batch experiment, kinetic and mechanism studies," *Bioresource Technology* 268, 149-157. DOI: 10.1016/j.biortech.2018.07.125

Zhou, B., Wang, Z., Shen, D., Shen, F., Wu, C., and Xiao, R. (2017). "Low cost earthworm manure-derived carbon material for the adsorption of Cu^{2+} from aqueous solution: Impact of pyrolysis temperature," *Ecological Engineering* 98, 189-195. DOI: 10.1016/j.ecoleng.2016.10.061

Article submitted: February 12, 2019; Peer review completed: April 7, 2019; Revised version received: April 11, 2019; Accepted: April 13, 2019; Published: April 18, 2019.
DOI: 10.15376/biores.14.2.4430-4453